MODELING AND EXPERIMENTAL INVESTIGATION OF PRE-MIXED MULTI-POWDER FLOW IN FABRICATING FUNCTIONAL GRADIENT MATERIAL BY LASER METAL DEPOSITION PROCESS

W. Li[a], J. W. Zhang[a], S. Karnati[a], Y. L. Zhang[a], F. Liou[a], J. Newkirk[b], K. M. B. Taminger[c], and W. L. Seufzer[c]

[a]Department of Mechanical and Aerospace Engineering, Missouri University of Science and Technology, Rolla, MO 65409, United States
[b]Department of Metallurgical Engineering, Missouri University of Science and Technology, Rolla, MO 65409, United States
[c]NASA Langley Research Center, Hampton, VA 23681, United States

Abstract

Laser Metal Deposition (LMD) is an effective process to fabricate Functionally Gradient Material (FGM) from pre-mixed powders. Since the supplied multi-powder directly affects the deposited FGM's composition, investigation on Pre-Mixed Multi-Powder (PMMP) flow during LMD is greatly needed. This paper presents a comprehensive numerical PMMP flow model. By solving discrete particle force balance equations coupled with continuity equations and momentum equations for carrier gas, the dynamic behavior of PMMP flow through powder feeder pipe and out of nozzle was calculated. To verify modeling results, pre-mixed Cu and 4047 Al powder was transported and patterned in an epoxy resin coating after exiting nozzle. The distribution of exiting pre-mixed powder was plotted by quantifying the volume percentages of different powders. The gathered distribution data was used to estimate the exiting pre-mixed powder's composition, and finally validate modeling results.

Keywords: Functionally Gradient Material; Pre-Mixed Multi-Powder; FGM composition; Numerical modeling.

Introduction

1. FGM and LMD

Functionally Gradient Material (FGM) is arousing more and more attention in the area of advanced material processing. FGM is characterized by the variation in composition and structure gradually over volume [1], resulting in corresponding gradual changes in the properties of the material as shown in Fig.1. FGM can be designed for specific functions and applications, and can combine two or three different materials into one structure and perform multiple functions [2]. FGM can cover various types of material transitions, such as metal to metal, metal to ceramics,

metal to biomaterial, ceramics to biomaterial, etc [3]. To fabricate the FGM structure, Laser Metal Deposition (LMD) is an effective process technique, in which gradually varying in composition over volume can be achieved by pre-designed multi-composition metallic powders. These powders are melted following specific routes, like straight lines, curves, zig-zag, etc, in order to manufacture the parts designed for customer's needs [4]. High cooling rate in LMD will bring refined microstructure size so that guaranteeing the enough material strength [5].
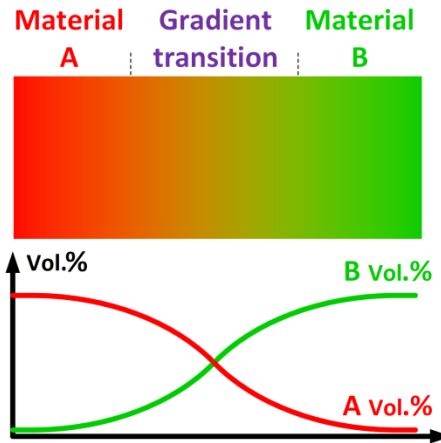

Fig.1. FGM structure: gradually varying composition over volume

A necessary factor in FGM manufacturing with LMD is the multi-composition powder. Based on the current powder processing techniques, pre-alloyed powder and pre-mixed powder are two basic sources. Pre-alloyed powder can provide precise chemical composition, which is the ideal powder input to manufacture the FGM structure. However, there are some limitations for the usage of pre-alloyed powder. First of all, FGM fabrication requires the chemical compositions in products keep changing. Pre-alloyed powder has the fixed chemical composition and cannot change anymore. It is only useful to fabricate some areas in FGM structure, but is very limited for the whole product. In addition, sometimes it is very hard to find pre-alloyed powder whose composition can match user requirements precisely. Secondly, the price of pre-alloyed powder is often expensive, so it is not good choice to control the manufacturing cost. Owing to the above reasons, pre-mixed powder is preferred because it is much more practical. The preparation of per-mixed powder is very easy to control. According to the composition requirement of FGM structure, several kinds of metal or elemental powders are weighed. Their weight percentages (wt.%) or volume percentages (vol.%) should match the required chemical composition ratio in FGM structure. Then all the powders are blended adequately by the mixing equipment. After that, the blended powder is used as the powder source for LMD process. The best merit of pre-mixed powder is the flexibility. Operators can obtain the powder source with any chemical composition ratio at any time, and adjust the composition of powder efficiently. In addition, because pre-mixed powder is from mixing some basic alloy or elemental powder, it is much better in saving fabrication cost than pre-alloyed powders.

2. Problem description

In the process of LMD fabricating FGM structure, the Pre-Mixed Multi-Powders (PMMP) are input into powder feeder. Inert argon gas flow with particular velocity drives the powders to move along the powder feeder pipe, then spray out into the melt pool through the nozzle. Since the multi-powders have different particle densities and sizes, under the same driving source from argon gas flow, the movements of multi-powders will be hard to keep uniform. In FGM manufacturing, the material composition ratio in any different area is required strictly. Non-uniform multi-powders movements will ruin the gradually varying material composition ratio, and further the wanted material performance in FGM. Fig.2 shows a research work in fabricating FGM structure of Ti6Al4V and TiB2. This experimental research work is introduced here because the powder separation issue was very obvious. Ti6Al4V was used as substrate. Pre-mixed Ti6Al4V and TiB2 powders were prepared with designed wt.% ratio (Ti6Al4V : TiB2= 30:1). The density and particle size of two types of powder were described in Table.1. Introducing of TiB2 will improve the modulus and strength of Ti6Al4V alloy. This improvement can be observed through the Vickers Hardness test Number (VHN). VHN of Ti6Al4V deposited with TiB2 should be bigger than the VHN of regular Ti6Al4V. Pre-mixed powders were deposited into a thin wall shape sample by CW fiber laser, which was schematically illustrated in Fig.2. Four thin wall samples were fabricated in sequence by LMD process to investigate the VHN's repeatability through employing same powder mixing design and same processing parameters. Center points of four samples were selected as Vickers hardness test points.

Particle	Density	Mean Size
Ti6Al4V	4.43 g/cm3	127 μm
TiB2	4.52 g/cm3	26 μm

- ● **Ti6Al4V particle**
- • **TiB2 particle**
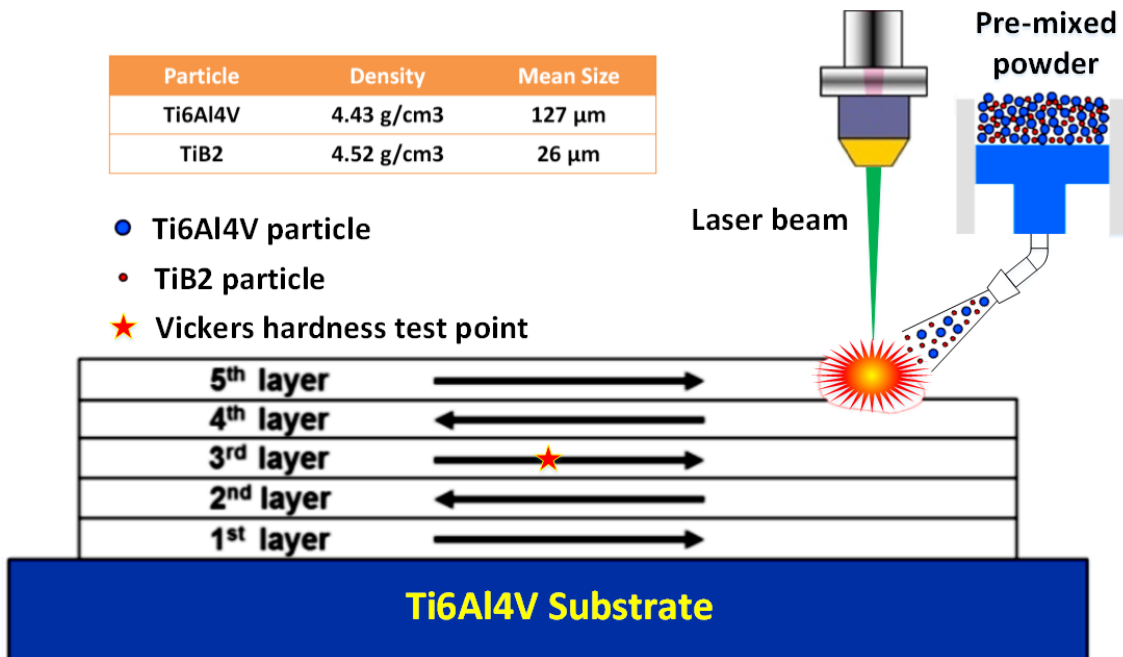- ★ **Vickers hardness test point**

Fig.2. Illustration of Ti6Al4V-TiB2 FGM fabrication with LMD

VHN comparison of four samples in sequence is shown in Fig.3a. From sample 1 to sample 4, VHN is observed as decreasing from 453 to 363. This result indicates the hardness of samples were not repetitive although the same pre-mixed powder and identical processing parameters were employed. Introducing TiB_2 can enhance the hardness of Ti6Al4V because TiB_2 is one type of ceramics with super high hardness. Decreasing VHNs of four samples indicates that consumed TiB_2 powder reduced in sequence from sample 1 to sample 4. This deduction was demonstrated by the optical microscopy images of mixed Ti6Al4V and TiB_2 powders in Fig. 4b-4d. Fig.3b shows the fresh mixed powders. Ti6Al4V particle is in the form of spherical ball with the mean diameter of 127 μm. TiB_2 particle is one type of ceramics with irregular shape. TiB_2 particle mean size is 26 μm which is much smaller than Ti6Al4V particle. In Fig. 4b, a lot of both particles can be observed clearly. Fig.3c shows the mixed powders after depositing first two samples and before 3rd deposition.
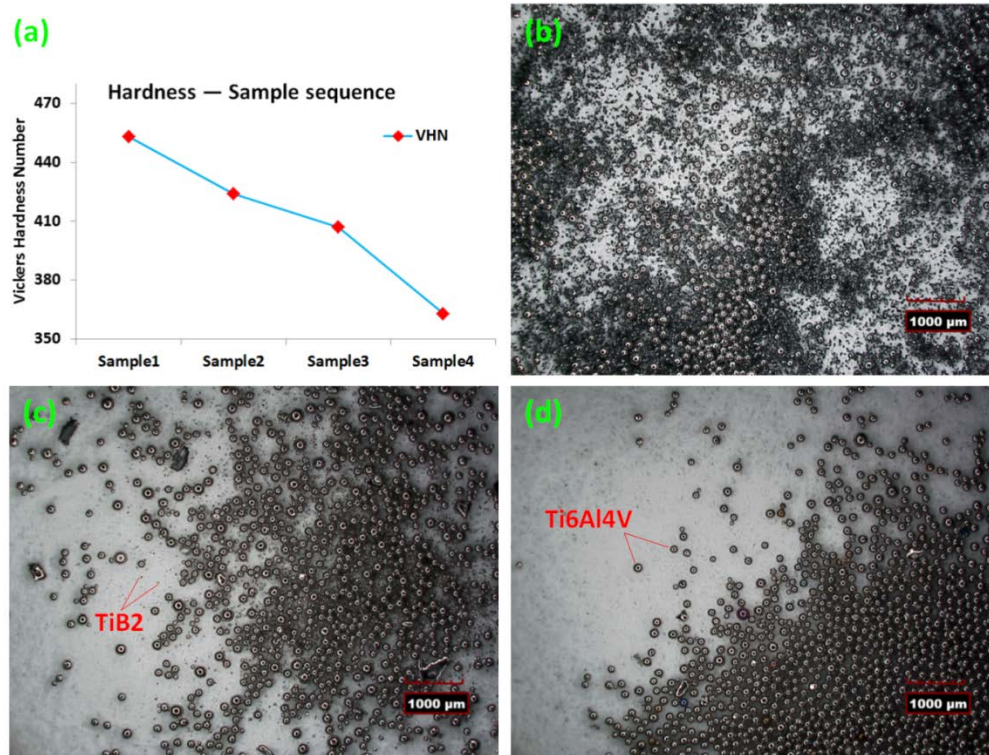

Fig.3. (a).VHN of four samples in sequence; (b). fresh mixed powders; (c). remaining mixed powders after prior two depositions; (d). remaining mixed powders after all the four depositions.

It is easy to find that the amount of TiB_2 reduced sharply comparing with the amount in fresh mixed powders. Fig.3d shows the mixed powders after all of four depositions. Almost no TiB_2 particle can be observed and only Ti6Al4V particle were left. Through comparing the optical microscopy images of mixed powder, the composition ratio of powders did not keep designed ratio in the process of LMD. In depositing the prior samples, the consumed TiB_2

powder was more than depositing latter samples. This caused the decreasing hardness as above mentioned. Since TiB2 particle was rich in fresh mixed powders, but became poor gradually, and almost vanished after all the depositions, it can be inferred that TiB2 particles moved faster than Ti6Al4V particle in powder feeder. This kind of inaccurate composition ratio of pre-mixed powders is becoming a critical issue in process of fabricating FGM structure through LMD. Therefore, an effective solution for this issue is urgently needed.

The issue of inaccurate composition ratio of pre-mixed powders is mainly caused by the particles movements in powder flow. In order to address this issue, investigation on PMMP flow during LMD is greatly needed. So far, there is no special research focusing on PMMP flow in fabricating FGM. Some previous research results all focused on the powder flow with identical material instead of mixed multi-component powders. Pinkerton and Li [6] developed a mathematical model relating to powder flow rate and powder feeder nozzle dimensions. In their study, stainless steel 316L powder was used to analyze the behavior of the axial powder stream concentration from a coaxial laser cladding nozzle. Pan and Liou [7] studied gravity-driven metal powder flow in coaxial nozzle for laser-aided direct metal deposition process with the H13 tool steel powder. Pan and Liou [8] also investigated the metallic powder flow in a coaxial nozzle for laser aided deposition process through numerical simulation method. Zekovic et.al [9] introduced a numerical simulation method to analyze gas-powder flow from radially symmetrical nozzles in laser-based direct metal deposition. Wen et.al [10] presented a comprehensive modeling method to predict the whole process of coaxial powder flow including the Stellite-6 particle stream flow in and after the powder feeder nozzle, and laser-particle interaction process. Tan et.al [11] developed a photographic system for the titanium powder feeding process of laser solid forming in which high speed camera, particle speed and powder flow concentration behaviors were described based on the powder flow images. Zhang et.al [12] used one numerical method to simulate the AISI420 steel powder flow field on coaxial powder nozzle in laser metal direct manufacturing process. More attentions were paid on analyzing the powder stream behavior through both numerical and experimental methods, but the powder particles in any of these studies were the same material.

So far, there is no special research to investigate the PMMP flow in LMD process. This study is to fill in this gap since supplied PMMP powder directly affects the deposited FGM's composition, which is an important factor in guaranteeing FGM structure performance. The purpose of this study is using modeling analysis to simulate the pre-mixed particle movement in the powder feeder pipe, so that provide a reasonable reference for FGM fabrication. In this study, a comprehensive numerical PMMP flow model was presented. By solving discrete particle force balance equations coupled with continuity equations and momentum equations for carrier gas, the dynamic behavior of PMMP flow through powder feeder pipe and out of nozzle was calculated. To verify modeling results, pre-mixed Cu and 4047 Al powder was transported and patterned in an epoxy resin coating after exiting nozzle. The distribution of exiting pre-mixed powder was

plotted by quantifying the volume percentages of different particles to estimate the exiting pre-mixed powder's composition, and finally validate modeling results.

Modeling of PMMP flow

1. Background description

A typical powder feeder configuration with supplied PMMP powder is schematically illustrated in Fig. 4. Different color dots indicate two different types of powders. With designed composition ratio, two types of powder are mixed together then supplied as powder source. In LMD process, inert argon gas flow plays the role of carrier to drive all types of powders to feed through powder feeder pipe and spray out to melt pool after leaving the nozzle. Suppose two types of particle are in the spherical shape. Because of different particle density and size, the driving force per each kind of particle is different. So the movements of powders will be hard to keep uniform. In FGM manufacturing, the material composition ratio in any different area is required strictly. Non-uniform multi-powders movements will make it hard to control the powder's ratio, and ruin the gradually varying material composition, and further the wanted material performance in FGM. The purpose of this study is to investigate the different particles' movements in powder feeder pipe through a comprehensive modeling. The simulation results were validated by pre-mixed powders feeding experiment.
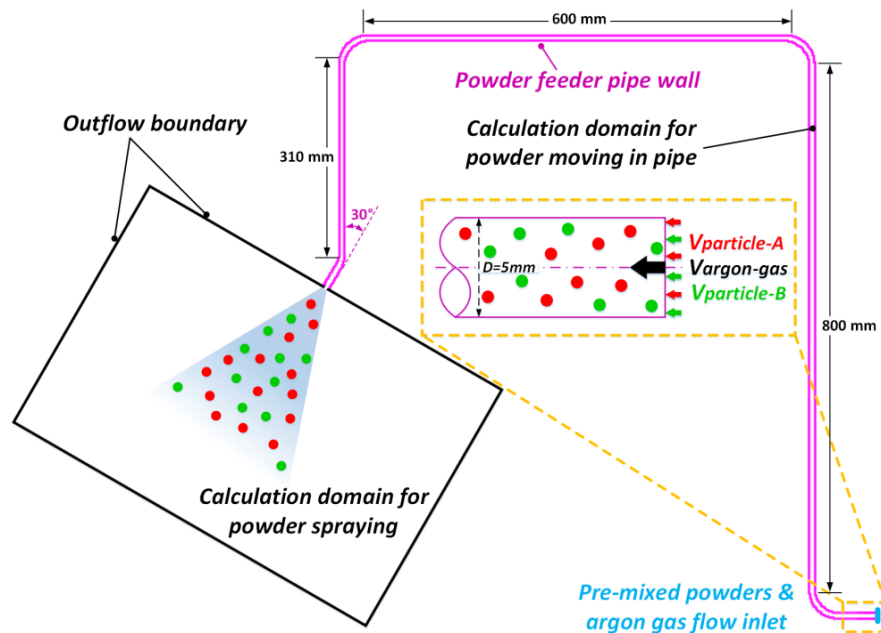

Fig.4. Typical powder feeder configuration with supplied PMMP powder and calculation domain.

2. Calculation Domain and boundary conditions

Fig.4 describes the 3-dimensional calculation domain used in the numerical model. The powder feeder pipe shape is designed like this in order to make the calculation domain close to the real experiment condition. The dimensions are described in Fig.4. The boundary condition of inlet was set as velocity inlet boundary, which was indicated with blue color. The velocities of argon gas flow and PMMP powder flow were employed at this boundary condition. Powder feeder pipe wall, which was indicated with magenta, was set as wall boundary condition. In computational fluid mechanics, wall means there is not any mass, flow, pressure passing through the wall. A calculation domain for powder spraying behavior was defined near the outlet nozzle of powder feeder pipe, whose boundary was indicated with black color. Outflow boundary condition was used surrounding the powder spraying domain. The outflow boundary is used to simulate the boundary condition where unknown outlet velocity and pressure happen but follow the developing process of fluid flow and conservation requirement. For the boundary of pipe wall, it is defined as wall boundary in fluid flow. Under this boundary condition, particle will be rebounded when it collides with wall. For the boundary of pipe outlet, it is defined as outflow boundary. Under this boundary condition, any mass can outflow freely. The direction of nozzle was leaning at 30 degree angle with the vertical pipe.

3. Solving techniques

As discussed above, the gas–powder flow is a complex two phase problem. In this study, the gas phase is treated as continuum, while the particle phase is simulated as a discrete phase that consists of two different particles dispersing in the continuous argon gas phase. The fluid behavior of continuous gas phase is modeled by solving the continuity equations and Navier–Stokes equations. The dispersed phase is solved by tracking a certain number of particles through the calculated domain. The trajectory of a discrete phase particle is solved by integrating the force balance on the particle, which is written in a Lagrangian reference frame [13]. The argon gas flow behavior in powder feeder pipe and near nozzle was simulated first by solving the continuity equations and Navier-Stokes equations. Then the acquired argon gas flow field was used as the input for simulating the PMMP particle flow. PMMP particle properties, including densities, size, shape, wt.% ratio, inlet velocity, were defined before calculation. Then powder flow field in the pipe and near the nozzle was simulated by coupling solving the interactions between the two phases and particle force balance equations. The coupling was accomplished by alternatively solving the continuous and discrete equations until the convergence for both phases. The employed governing equations are described in next section. The modeling work in this research was solved by commercial solver Fluent 14.0.

4. Governing equations

4.1. Argon gas turbulence flow

Due to the gas-particle interaction behavior, the argon gas flow in powder feeder pipe is characterized by the turbulence, a turbulent model was built to solve the dynamic fluid behavior of argon gas phase. The PMMP particles motions were calculated based on the acquired argon gas flow field. The turbulence model includes three types of equations: continuity equation of mass; momentum conservation equations, and $k - \varepsilon$ kinetic energy equations. The calculation domain for argon gas phase described in section2 is axisymmetric, steady, and turbulent continuous gas flow with homogeneous chemical composition and no body force or swirl velocity [10], the governing equations are present as follows [14] [15]:

Continuity equation of argon gas mass:

$$\frac{\partial(\rho u_j)}{\partial x_j} = 0 \tag{1}$$

where ρ is the density of argon gas, u_j is the velocity vector along the jth direction. Because of the axisymmetric calculation domain, u_j should be decomposed to axial velocity vector u_x and radial velocity vector u_r. Therefore, the argon gas mass continuity conservation equation is deduced as:

$$\frac{\partial(\rho u_x)}{\partial x} + \frac{1}{r}\frac{\partial(r\rho u_r)}{\partial r} = 0 \tag{2}$$

Where x and r are the axial and radial coordinate, respectively.

The momentum conservation equation in the axial direction:

$$\frac{\partial(\rho u_x u_x)}{\partial x} + \frac{1}{r}\frac{\partial(r\rho u_r u_x)}{\partial r} = -\frac{\partial p}{\partial x} + \frac{1}{r}\frac{\partial}{\partial x}\left[r\mu\left(2\frac{\partial u_x}{\partial x} - \frac{2}{3}(\nabla \cdot \vec{u})\right)\right] + \frac{1}{r}\frac{\partial}{\partial r}\left[r\mu\left(\frac{\partial u_x}{\partial r} + \frac{\partial u_r}{\partial x}\right)\right]$$
$$+ \phi_x \tag{3}$$

The momentum conservation equation in the radial direction:

$$\frac{\partial(\rho u_x u_r)}{\partial x} + \frac{1}{r}\frac{\partial(r\rho u_r u_r)}{\partial r} = -\frac{\partial p}{\partial r} + \frac{\partial}{\partial x}\left[\mu\left(\frac{\partial u_x}{\partial r} + \frac{\partial u_r}{\partial x}\right)\right] + \frac{1}{r}\frac{\partial}{\partial r}\left[r\mu\left(2\frac{\partial u_r}{\partial r} - \frac{2}{3}(\nabla \cdot \vec{u})\right)\right]$$
$$- 2\mu\frac{u_r}{r^2} + \frac{2}{3}\frac{\mu}{r}(\nabla \cdot \vec{u}) + \phi_r \tag{4}$$

where ∇ is the Hamilton operator, μ is the effective dynamic viscosity of the continuous argon gas.

$$\nabla \cdot \vec{u} = \frac{\partial u_x}{\partial x} + \frac{\partial u_r}{\partial r} + \frac{u_r}{r} \tag{5}$$

In Eqs. (3) and (4), the source term ϕ_i $(i = x, r)$ represents the coupled momentum transport from the particle phase:

$$\phi_i = \frac{1}{V_c} \sum_{j=1}^{n_c} \frac{3\mu C_D Re}{4\rho_p d_p^2} (u_{p,i} - u_i) \dot{m}_p^j \Delta t^j \tag{6}$$

where V_c is the volume of one cell C; $\dot{m}_p^j$ is the particle mass rate for the jth trajectory passing through this cell; n_c is the total number of particle trajectories passing through the cell; Re and C_D are the Reynolds number and the drag coefficient of one particle; ρ_p, d_p, and $u_{p,i}$ are the density, diameter, and velocity in direction of one particle, respectively[10].

The turbulence flow in powder feeder pipe requires appropriate modeling procedure to describe the turbulent fluctuation effects on particle movements. The most popular turbulent model is the standard $k - \varepsilon$ model which is proposed by Launder and Spalding[16]. The turbulence behavior is described through introducing two additional variables: the turbulent kinetic energy k, and the viscous dissipation rate of turbulent kinetic energy ε. Serag-Eldin and Spalding [14] provided detailed description and expressions for these two variables. The standard $k - \varepsilon$ model is used to simulate the argon gas flow in powder feeder pipe.

Considering the axisymmetric calculation domain, the conservation of kinetic energy of turbulence is:

$$\frac{\partial(\rho u_x k)}{\partial x} + \frac{1}{r}\frac{\partial(r\rho u_r k)}{\partial r} = \frac{\partial}{\partial x}\left[\left(\mu_l + \frac{\mu_t}{\sigma_k}\right)\frac{\partial k}{\partial x}\right] + \frac{1}{r}\frac{\partial}{\partial r}\left[r\left(\mu_l + \frac{\mu_t}{\sigma_k}\right)\frac{\partial k}{\partial r}\right] + G_k - \rho\varepsilon \tag{7}$$

The conservation of the viscous dissipation rate of turbulent kinetic energy is:

$$\frac{\partial(\rho u_x \varepsilon)}{\partial x} + \frac{1}{r}\frac{\partial(r\rho u_r \varepsilon)}{\partial r} = \frac{\partial}{\partial x}\left[\left(\mu_l + \frac{\mu_t}{\sigma_\varepsilon}\right)\frac{\partial \varepsilon}{\partial x}\right] + \frac{1}{r}\frac{\partial}{\partial r}\left[r\left(\mu_l + \frac{\mu_t}{\sigma_\varepsilon}\right)\frac{\partial \varepsilon}{\partial r}\right] + C_1 G_k \frac{\varepsilon}{k} - C_2\rho\frac{\varepsilon^2}{k} \tag{8}$$

$$\mu = \mu_l + \mu_t ; \quad \mu_t = \rho C_\mu k^2/\varepsilon \tag{9}$$

where μ_l and μ_t represent the laminar and turbulent viscosity. They are solved by the Eq. (9). G_k is the rate of production of kinetic energy. The model constants have five constants C_1, C_2, C_μ, σ_k, and σ_ε, which have following default values [16]. These default values have been determined for fundamental turbulent flows including frequently encountered shear flows like boundary layers, mixing layers and jets as well as for decaying isotropic grid turbulence [15].

$$C_1 = 1.44;\ C_2 = 1.92;\ C_\mu = 0.09;\ \sigma_k = 1.0;\ \sigma_\varepsilon = 1.30 \tag{10}$$

4.2. Particle flow

The two-phase flow problem involving the trajectory of a dispersed particle phase is solved by integrating the force balance on the particle in a Lagrangian reference frame. The dynamic governing equations for each particle are written as follows[10].

$$\frac{d\vec{x}}{dt} = u_p \tag{11}$$

$$\frac{du_p}{dt} = \frac{18\mu}{\rho_p d_p^2} \frac{C_D Re}{24} (u - u_p) + \frac{g(\rho_p - \rho)}{\rho_p} \tag{12}$$

$$Re = \frac{\rho d_p |u - u_p|}{\mu} \tag{13}$$

where u_p, ρ_p, and d_p are the velocity, density, and diameter of each particle, respectively. Eq.(12) indicates that the particles are basically driven by the main forces of both gas flow drag and gravity. C_D is the drag coefficient which is expressed with four coefficients [7].

$$C_D = \frac{24}{Re}(1 + b_1 Re^{b_2}) + \frac{b_3 Re}{b_4 + Re} \tag{14}$$

$$b_1 = \exp(2.3288 - 6.4581\varphi + 2.4486\varphi^2)$$

$$b_2 = 0.0964 + 0.5565\varphi \tag{15}$$

$$b_3 = \exp(4.905 - 13.9844\varphi + 18.4222\varphi^2 - 10.2599\varphi^3)$$

$$b_4 = \exp(1.4681 + 12.2584\varphi - 20.7322\varphi^2 + 15.8855\varphi^3)$$

The four efficient are the functions of shape factor φ. In modeling particle movement and fluid behavior, it is necessary to consider the shape effect of the particles in terms of shape factor φ, since it describes how spherical a particle is [15]. In Eq.(16), shape factor is expressed as the ratio of s and S. s is the surface area of a sphere which has the same volume as the particle. S is the actual surface area of the particle [15]. The shape factor is equal to one for a spherical particle, and always less than one for non-spherical particles[10]. In this research, two types of particles were employed. Cu particle shape is very close to spherical shape (in Fig.5a), so its shape factor is defined as 1. 4047 Al particle shape is satelliting shape (in Fig.5b), so its shape factor value is defined as 0.8 according to Pan [7].

$$\varphi = \frac{s}{S} \tag{16}$$

5. Particle description

In order to observe the dynamic behavior of PMMP flow through powder feeder pipe and out of nozzle, pure Cu powder and 4047 Al powder were used in this research. There are two reasons of choosing these two powders. First of all, Cu particle is red or close to red, while 4047 Al is of gray color. Color difference can make it easy to differentiate these two particles in the experiments. Secondly, the density of Cu particle is 8.94 g/cm, while 4047 Al's density is only 2.6 g/cm. Cu density is approximately three times of 4047 Al density. According to eq.12, particle acceleration is in reverse proportion to particle density. Significant difference in density will cause the particle acceleration difference. So the separation of PMMP flow in powder feeder pipe may be easy to observe.

Fig.5 describes the two particles through optical microscope images. The particles size distributions for the two types of powder were displayed by the sieve analysis in Table.1and Table.2. For pure Cu powder, most of particles show as spherical shape. More than 80% particles diameters are in the range of 45-106 μm. In addition to this, 3.7% Cu particles diameters are 106-125μm. The remaining Cu particles diameters are in the range of 125-212 μm. 4047 Al powder show as satelliting shape. Close to 30% particles diameters are from 45 to 75 μm. There are more than 40% particles whose diameters are in the range of 75 to 106 μm. Then about 20% particle diameters are in the range of 106 to 125μm. 5% particles diameters are 125-150μm. Some less amount of particles are larger than 150 μm.
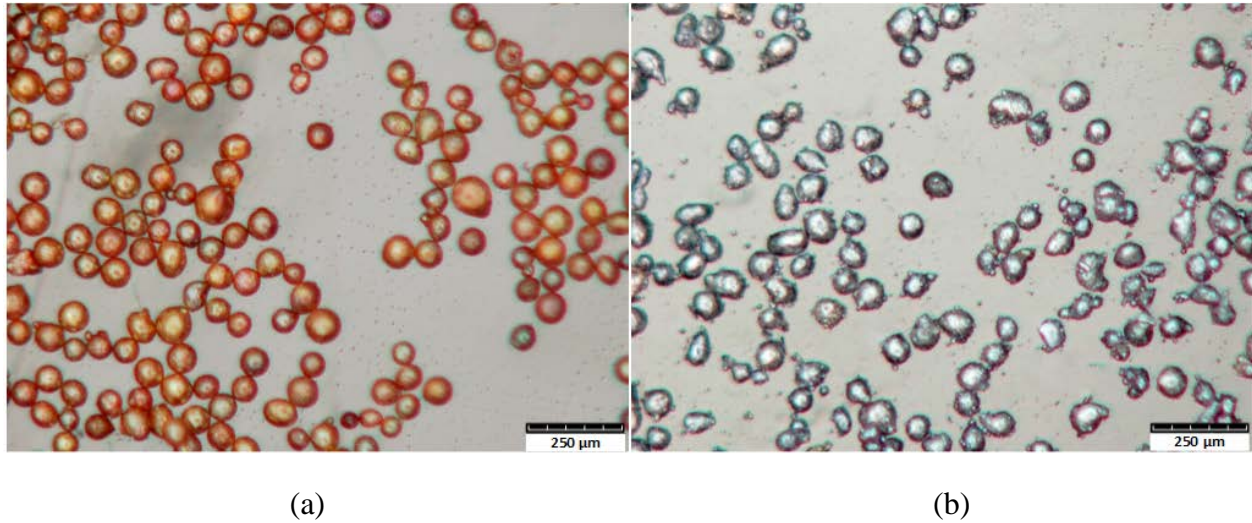
<center>(a)   (b)</center>

Fig.5. Optical microscopic images for: (a) Cu particles; and (b) 4047 Al particles.

Table.1. Sieve analysis of pure Cu powder

Sieve type	70 mesh	100 mesh	120 mesh	140 mesh	200 mesh	325 mesh
Size (μm)	>212	150-212	125-150	106-125	75-106	45-75
Percentage (%)	0.0	1.3	2.4	3.7	47.4	45.2

Table.2. Sieve analysis of 4047 Al powder

Sieve type	70 mesh	100 mesh	120 mesh	140 mesh	200 mesh	325 mesh
Size (μm)	>212	150-212	125-150	106-125	75-106	45-75
Percentage (%)	1.1	2.8	5.4	20.3	42.5	27.9

6. Modeling result and discussion

6.1. Operating parameters

The operating parameters in the modeling process were set as in Table 3. The 4047 Al and Cu powder were mixed with same volume percentage ratio (vol.% =50%) before the process. The powder feeding rates for 4047 Al and Cu were 1.1 g/min and 3.29 g/min, respectively. The carrier argon gas flow rate was 10 SCFH. The pipe filled with pre-mixed powders from the beginning with the same initial velocity with argon gas. According to Eq.(12), the particle with bigger size and heavier density will have smaller acceleration. In order to observe the particle separation clearly, bigger Cu particle (75-106μm) and smaller 4047 Al particle (45-75μm) were selected in this work. The total simulation time was 25 s.

<center>297</center>

Table.3. The operating parameters in the simulation

Operating parameters	Value
Vol.% ratio	50%:50%
4047 Al powder feed rate	1.1 g/min
Cu powder feed rate	3.29 g/min
Argon gas flow rate	10 SCFH
4047 Al particle diameter	45-75 μm
Cu particle diameter	75-106 μm
Simulation time	25 s
Time step size	0.01s
Cu density	8.94 g/cm^3
4047 Al density	2.6 g/cm^3

6.2. PMMP stream structure

Fig.6 depicts the simulated PMMP stream structure formed by multi-particle trajectories. Blue color is used to indicate 4047 Al particle trajectory. Red color expressed Cu particle trajectory. It can be seen that the powder flow starts to expand at the exit of powder feeder nozzle. The expansion is mainly caused by the carrier gas's driving force and gravity. During the particle's moving in the powder feeder pipe, two moments were selected: t_a=0.5s, t_b=1s. At the two moments, the PMMP particle distributions were both described in Fig.6. Cu particle density is approximately three times of 4047 Al particle. What is more, Cu particle size is bigger than 4047 Al particle. On the basis of Eq.(12), particle acceleration is roughly inverse proportion to the product of particle density and particle diameter square. Therefore, 4047 Al particle will have bigger acceleration, because it is lighter and smaller. On the other hand, Cu particle will have smaller acceleration since it is heavier and bigger. When the pre-mixed 4047 Al and Cu particle enter the powder feeder pipe, the initial velocity can be regarded as zero. They are carried by argon gas flow to move in the powder feeder pipe. Larger acceleration will result in the larger moving velocity, so the separation of different types of particle will be caused. By tracking Cu and 4047 Al particles, it was observed in simulation result that pre-mixed powder separated at t=1s very clearly, and the pre-mixed powder stayed in mixing at t=0.5s. These two moments were selected because the mixing and separation were easy to be observed. In Fig.6, it can be found that at the moment of t_a=0.5s, both types of particles are moving neck and neck. But at the moment of t_b=1s, some 4047 Al particle (blue point) are moving ahead of Cu particle (red point). This phenomenon illustrates that PMMP particle will gradually separate when they are moving in the powder feeder. The composition ratio is designed in PMMP particle before the LMD process. However, the actual composition in the deposited part will be defaulted and influenced by the separation of PMMP particle flow.
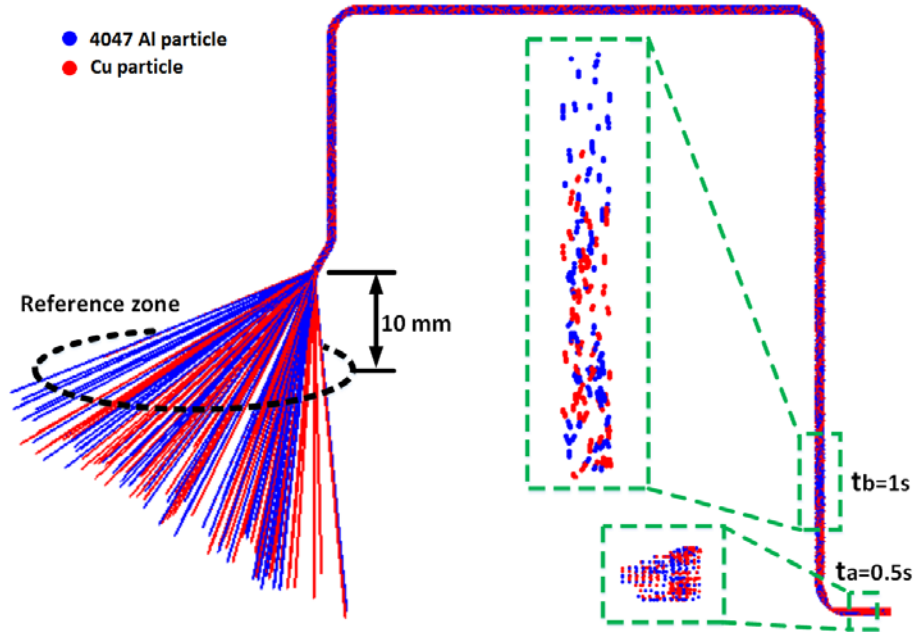
Fig.6. Simulated PMMP powder flow structure

6.3. Quantification of PMMP particle separation behavior

In order to quantify the PMMP particles' separation behavior, a circular reference zone was defined in Fig.6. This circular surface was horizontal, whose diameter was large enough to encompass all the particles spraying out from the nozzle. The perpendicular distance between the reference zone and nozzle was 10 mm. This definition was designed to match the experiment set-up. The quantification of PMMP particle separation was achieved through analyzing the particle number and relative volume percentage in the reference zone at specified moments. Eleven moments were specified as: t_i=5s, 7s, 9s, 11s, 13s, 15s, 17s, 19s, 21s, 23s, and 25s, where i=1~11. At each moment, the numbers of different types of particle in the reference zone were counted then converted to the volume percentage (vol.%) of 4047 Al and Cu powder. The conversion process are described in Eq.(17) and Eq.(18).

$$Vol_{powder} = N_{particle} \times \frac{4}{3}\pi r_{mean}^3 \tag{17}$$

$$Vol.\%_{powder1} = 100 \times \frac{Vol_{powder1}}{Vol_{powder1} + Vol_{powder2}} \tag{18}$$

where Vol_{powder} indicates one type of powder's volume; $N_{particle}$ is the number of this type of particle in the reference zone. The particle diameter distribution is assumed as the Gaussian

distribution. r_{mean} is the mean radius, or the mathematical expectation value of the particle radius.

The predicted volume percentages of 4047 Al and Cu powder were shown in Fig. 7. As seen in Fig.7, blue diamond dot indicates the vol.% of 4047 Al powder, while red diamond represents the vol.% of Cu powder. It can be seen that 4047 Al particle came out first from the nozzle comparing with the Cu particle. This can be explained by the particle acceleration analysis in Section 4. 4047 Al particle's larger acceleration drove it to move faster than Cu particle. 4047 Al powder's vol.% experiences a gradual decrease along with time before the moment t=17s. This is because Cu particles gradually spray out from the nozzle so Cu powder covers some volume percentage. It is worth to note that after the moment of t=17s, both powders' vol.% tend to become stable, but both of volume percentages are different. 4047 Al powder volume percentage is approximately 20% bigger than Cu powder. In spite of same initial vol.% (50%) for the two powders, the different accelerations of particles and the relative separation of pre-mixed powder flow results in the volume percentage difference between two powders. Although both powders spray out simultaneously from the nozzle, 4047 Al particles' larger velocities cause more of them reaching the reference zone than Cu particles. In addition to volume percentage difference, another important result is both powders' volume percentages fluctuate slightly after stabilization. This is due to the gas-particle interaction behavior. The argon gas flow in powder feeder pipe is characterized by the turbulence. The local unsteady velocity fields in the turbulence result in the heterogeneous distribution of PMMP particles in powder feeder pipe and near the nozzle, furthermore cause the fluctuation of powders' volume percentages.
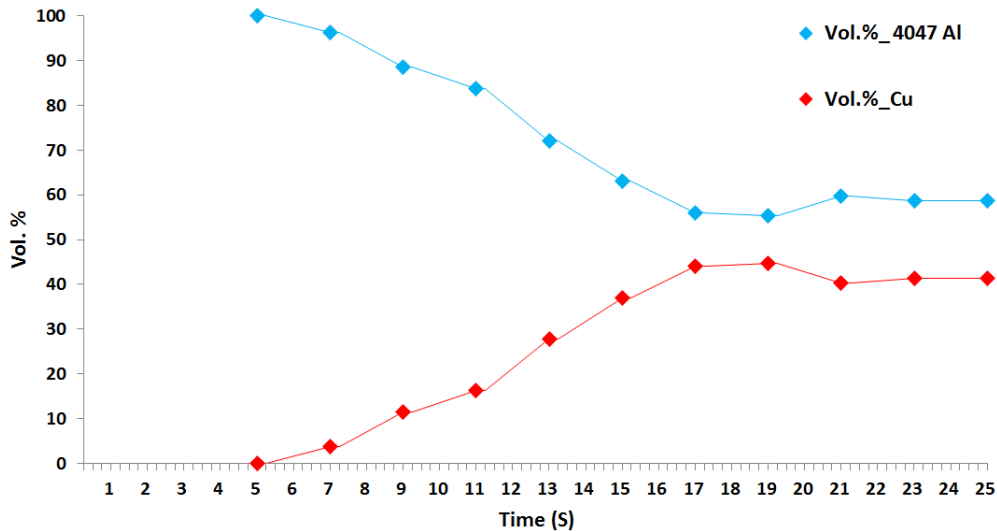

Fig.7. Predicted volume percentages of 4047 Al and Cu powder

Experiment validation

1. Experiment set-up

An experiment was carried out to validate the simulated results. The experiment set-up is schematically shown in Fig.8. A commercial powder feeder (Bay State Surface Technologies, Inc, Model-1200) was used to supply PMMP powder. The powders used in this experiment were prepared as: 4047 Al (45-75 μm) and pure Cu (75-106 μm), which are described in previous section. A plastic pipe, with 1.5 m in length and 5 mm in inner diameter, delivers the PMMP powder. Two linear motors (AEROTECH, Inc, Model-100SMB2) were employed to generate moving path. A piece of aluminum alloy plate, paved with sticky epoxy resin, was fixed on the linear motor to follow the generated path. The idea of this experiment is to use the sticky epoxy resin layer to collect the pre-mixed 4047 Al and Cu powders spraying out from the nozzle. The optical microscopy was used to observe the PMMP powder adhered on epoxy resin layer, then compare with the simulation result. The time of spraying powder was 25 s, which matches the time in the model. During this time range, powder feeder nozzle was moving above the epoxy resin layer following the specified path. After the epoxy resin was solidified, the collected PMMP powder was contained in it to form the particle pattern, then for the further observation. All the other operating parameters are same with the modeling definition.
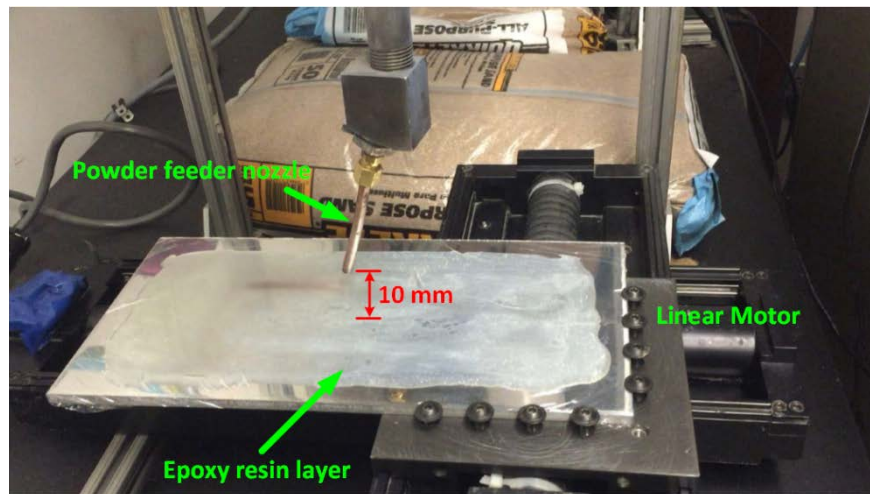

Fig.8. Experiment set-up

2. Experiment results and comparing with modeling results

After the sticky epoxy resin solidified, the PMMP particle pattern was ready for further observation. The experiment result was shown in Fig.9. It can be seen that gray 4047 Al particles and red Cu particles distribute in the solidified epoxy resin. An observation zone, which is indicated by a yellow rectangle in Fig.9, was defined with the size of 1.66 mm×1.24mm. All the particles in this observation zone were counted. Based on the counted number of both particles, volume percentages of both powders were converted using the Eq.(17) and Eq.(18).
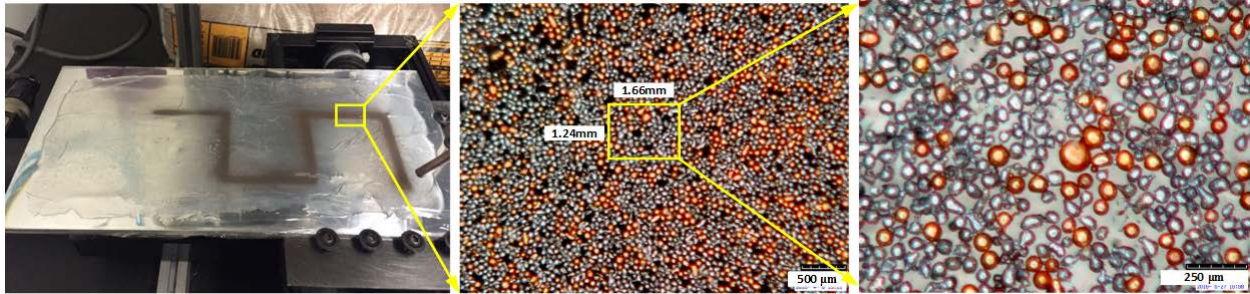
Fig.9. Experiment results and observation zone

To validate the modeling, four PMMP particle pattern samples were observed. These samples were chosen at the moments: t=11s, 15s, 19s, and 23s respectively. Fig. 10 shows you the optical microscopy images of the four particle pattern samples. By observing the image, it is clear that with the increase over time, more Cu particles were found in the sample. So the Cu powder vol.% will increase coupled with decreasing 4047 Al vol.%.
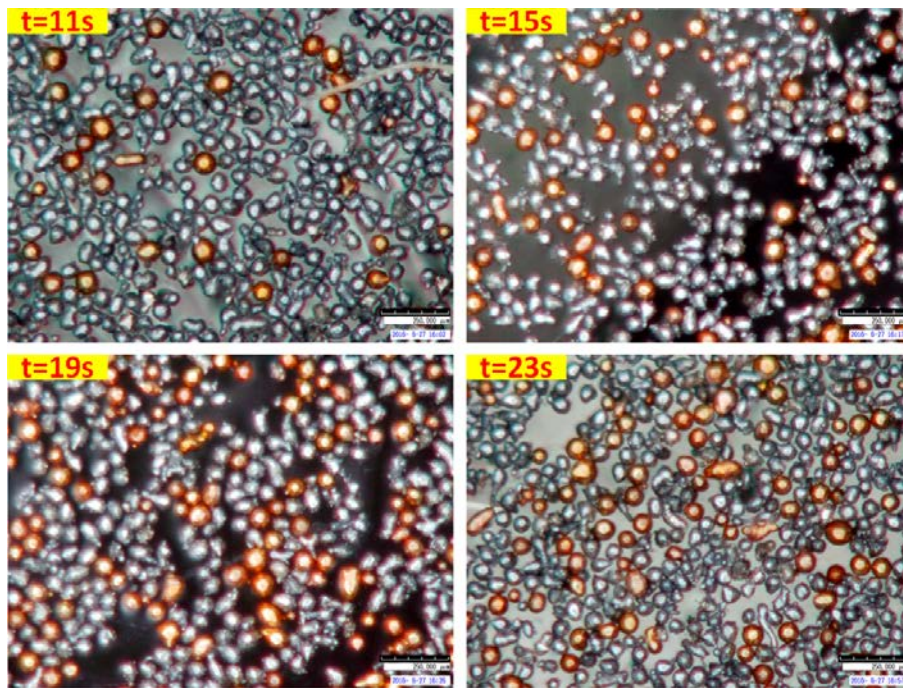

Fig.10. Four PMMP particle pattern samples

In Fig.11, the volume percentages of 4047 Al and Cu powder at the four samples were compared with the predicted volume percentages at the corresponding moments in modeling. Both of the modeling predictions and experimental results show clear trends. Due to heavier density and larger particle size, Cu particle's acceleration was smaller than 4047 Al particle.

Comparing Fig.11a and Fig.11b, 4047 Al powder vol.% is more than Cu powder. Both modeling and experimental results demonstrate this point. 4047 Al powder's vol.% experiences a gradual decrease then stabilization along with time. Because Cu particles gradually spray out from the nozzle, Cu powder volume percentage gradually increases then achieves to stabilization. Although same initial vol.% (50%) for the two powders were set, the experimental results show that the final stabilized volume percentages are different. It is worth to note that at the moment t=11s, the volume percentage difference of modeling prediction and experimental result is bigger than other three moments. At this moment, the experimental data of Cu powder volume percentage is remarkably more than the modeling predicted value. The reason should be attributed to the sifting error of sieves. When sifting the Cu powder, the sieves were used repeatedly. Some meshes in sieves were blocked by bigger Cu particles. So some amount of smaller Cu particles was hard to go through the blocked meshes so that they stayed. These smaller Cu particles had larger acceleration than other Cu particle. Therefore, they sprayed out from nozzle earlier than the expectation.
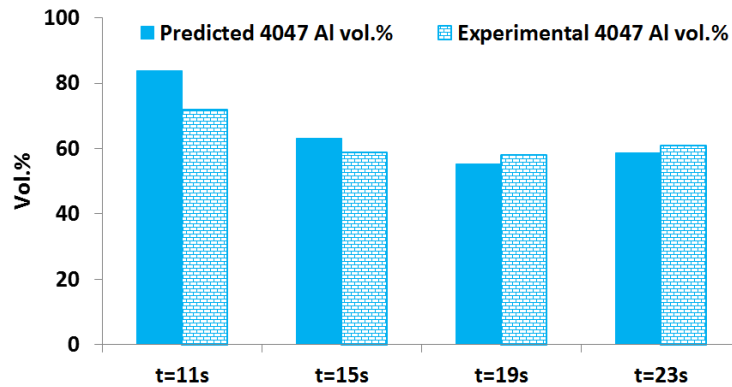
(a)
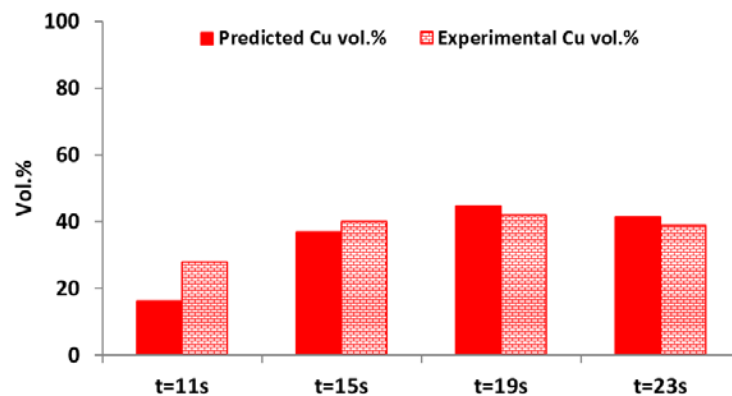
(b)

Fig.11. Comparison of predicted powder vol.% and experimental data for: (a) 4047 Al; (b) Cu powder.

Conclusion

A comprehensive numerical model that describes the dynamic behavior of Pre-Mixed Multi-Powder (PMMP) flow through powder feeder pipe and out of nozzle has been presented. By solving discrete particle force balance equations coupled with continuity equations and momentum equations for carrier gas, the dynamic behavior of PMMP flow was calculated. Predicted volume percentages (vol.%) of different powders have been validated by the experimental results. The modeling results show that 4047 Al particle came out first from the nozzle comparing with the Cu particle. This is because 4047 Al particle's larger acceleration drove it to move faster than Cu particle. 4047 Al powder's vol.% experiences a gradual decrease coupled with increasing Cu powder vol.%. Along with the time, both powders' vol. % tends to become stable, but both are different. 4047 Al powder vol.% is approximately 20% bigger than Cu powder in spite of same initial vol.% (50%) for the two powders. The argon gas turbulence flow results in the fluctuation of powders' volume percentage. The predicted values agree with the experimental data well. Due to the sifting error of sieves, in the beginning stage, the experimental data of Cu powder volume percentage is remarkably more than the modeling predicted value.

Reference

[1] Rabin, B., and Shiota, I., 1995, "Functionally Gradient Materials," MRS bulletin, 20(01), pp. 14-18.
[2] Yumin, Z., Xiaodong, H., and Jiecai, H., 1998, "Functionally Gradient Materials," Aerospace Materials & Technology, 28(5), pp. 5-10.
[3] HUANG, J.-d., WU, J., WANG, Y.-p., and HUANG, Q.-a., 2002, "Functionally Gradient Materials," Materiais Protection, 12, p. 002.
[4] Labudovic, M., Hu, D., and Kovacevic, R., 2003, "A three dimensional model for direct laser metal powder deposition and rapid prototyping," Journal of materials science, 38(1), pp. 35-49.
[5] Dinda, G., Dasgupta, A., and Mazumder, J., 2009, "Laser aided direct metal deposition of Inconel 625 superalloy: microstructural evolution and thermal stability," Materials Science and Engineering: A, 509(1), pp. 98-104.
[6] Pinkerton, A. J., and Li, L., "A verified model of the behaviour of the axial powder stream concentration from a coaxial laser cladding nozzle," Proc. Proceedings of ICALEO.
[7] Pan, H., Sparks, T., Thakar, Y. D., and Liou, F., 2006, "The investigation of gravity-driven metal powder flow in coaxial nozzle for laser-aided direct metal deposition process," Journal of manufacturing science and engineering, 128(2), pp. 541-553.

[8] Pan, H., and Liou, F., 2005, "Numerical simulation of metallic powder flow in a coaxial nozzle for the laser aided deposition process," Journal of Materials Processing Technology, 168(2), pp. 230-244.

[9] Zekovic, S., Dwivedi, R., and Kovacevic, R., 2007, "Numerical simulation and experimental investigation of gas–powder flow from radially symmetrical nozzles in laser-based direct metal deposition," International Journal of Machine Tools and Manufacture, 47(1), pp. 112-123.

[10] Wen, S., Shin, Y., Murthy, J., and Sojka, P., 2009, "Modeling of coaxial powder flow for the laser direct deposition process," International Journal of Heat and Mass Transfer, 52(25), pp. 5867-5877.

[11] Tan, H., Zhang, F., Wen, R., Chen, J., and Huang, W., 2012, "Experiment study of powder flow feed behavior of laser solid forming," Optics and Lasers in Engineering, 50(3), pp. 391-398.

[12] Zhang, A., Li, D., Zhou, Z., Zhu, G., and Lu, B., 2010, "Numerical simulation of powder flow field on coaxial powder nozzle in laser metal direct manufacturing," The International Journal of Advanced Manufacturing Technology, 49(9-12), pp. 853-859.

[13] Deen, N., Annaland, M. V. S., Van der Hoef, M., and Kuipers, J., 2007, "Review of discrete particle modeling of fluidized beds," Chemical Engineering Science, 62(1), pp. 28-44.

[14] Serag-Eldin, M., and Spalding, D., 1979, "Computations of three-dimensional gas-turbine combustion chamber flows," Journal of Engineering for Power, 101(3), pp. 326-336.

[15] Guide, A. F. U., 2011, "Release 14.0, ANSYS Fluent User Manual," Inc., November.

[16] Launder, B. E., and Spalding, D. B., 1972, "Lectures in mathematical models of turbulence."